Enhanced and Stable Field Emission from in Situ Nitrogen-Doped Few-Layered Graphene Nanoflakes

Navneet Soin,[†] Susanta Sinha Roy,*,[†] Soumyendu Roy,[‡] Kiran Shankar Hazra,[‡] Devi S. Misra,[‡] Teck H. Lim,[§] Crispin J. Hetherington,[§] and James A. McLaughlin[†]

[†]Nanotechnology and Integrated Bioengineering Centre (NIBEC), University of Ulster at Jordanstown, Shore Road, Newtownabbey BT37 0QB, United Kingdom

[‡]Department of Physics, Indian Institute of Technology (IIT) Bombay, Mumbai-400076, Maharashtra, India

[§]Department of Materials, University of Oxford, Parks Road, Oxford OX1 3PH, United Kingdom

ABSTRACT: Vertically aligned few-layered graphene (FLG) nanoflakes were synthesized on bare silicon (Si) substrates by a microwave plasma enhanced chemical vapor deposition method. In situ nitrogen (N_2) plasma treatment was carried out using electron cyclotron resonance plasma, resulting in various nitrogen functionalities being grafted to the FLG surface. Compared with pristine FLGs, the N_2 plasma-treated FLGs showed significant improvement in field emission characteristics by lowering the turn-on field (defined at 10 $\mu A/cm^2$) from 1.94 to 1.0 V/μm. Accordingly, the field emission current increased from 17 $\mu A/cm^2$ at 2.16 V/μm for pristine FLGs to about 103 $\mu A/cm^2$ at 1.45 V/μm for N-doped FLGs. Furthermore, N-doped FLG samples retained 94% of the starting current over a period of 10 000 s, during which the fluctuations were of the order of ±10.7% only. The field emission behavior of pristine and N_2 plasma-treated FLGs is explained in terms of change in the effective microstructure as well as a reduction in the work function as probed by X-ray photoelectron valence band spectroscopy.
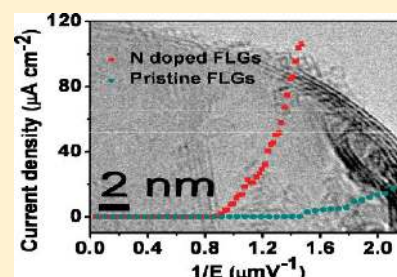
INTRODUCTION

Field emission (FE) has been extensively explored from various exotic low dimensional carbon nanomaterials, such as amorphous carbon films,[1] single and multiwalled carbon nanotubes (CNTs),[2] tubular graphitic cones,[3] vertically aligned nanowalls,[4] few-layered graphene (FLG) nanoflakes,[5,6] and, more recently, from doped and pristine graphene.[7,8] Graphene, a two-dimensional monatomic plane layer of hexagonally arrayed sp^2-hybridized carbon atoms forms the backbone of all the above-mentioned carbon nanostructures.[9] The highly desirable properties of graphene, such as atomic thickness, excellent electrical conductivity, and high aspect ratio, make it an ideal candidate for field emission applications.[7−9] Also, as compared to CNTs, the presence of a large number of edges may render graphene superior for electron tunneling.[7] Although FE in CNTs is highly efficient, it has been shown that heteroatom doping by elements, such as nitrogen, can further reduce the effective tunneling potential barrier, thereby reducing the turn-on field and significantly increasing the electron emission current.[10,11] Nitrogen acts as an electron donor in CNTs because it has five valence electrons and causes a shift in the Fermi level (E_F) to the conduction band and increases the electron density of states (DOS). In the case of graphene, theoretical studies have shown that substitutional heteroatom doping can modulate the band structure of graphene, leading to a metal−semiconductor transition, thereby expanding the applications of graphene.[12,13]

Although Malesevic et al.[5] and Qi et al.[6] have shown the field emission behavior of pristine and Ar plasma-treated FLG nanoflakes, respectively, to the best of our knowledge, until now, there have been no reports of field emission from heteroatom-doped vertically aligned FLG nanoflakes. We have recently reported on the synthesis and possible growth mechanism of vertically aligned FLG nanoflakes on bare silicon substrates using an MPECVD system.[14] The resultant morphology of the optimized structure, with terminal atomically thin layers and a robust physical structure, makes it an ideal candidate for the exploration of field emission properties. In situ nitrogen (N_2) plasma treatment of pristine FLGs was carried out using a room-temperature, low-pressure electron cyclotron resonance (ECR) plasma system. The change in the microstructure and chemical bonding of the FLGs upon N_2 plasma treatment was studied using a variety of techniques, such as Raman spectroscopy, transmission electron microscopy (TEM), and X-ray photoelectron spectroscopy (XPS). The influence of N_2 plasma treatment and its role in field emission characteristics of FLGs is discussed in detail.

EXPERIMENTAL SECTION

The synthesis of FLGs was carried out in a SEKI MPECVD deposition system, equipped with a 1.5 kW, 2.45 GHz microwave source. The substrates used were bare n-type heavily doped Si wafers (resistivity < 0.005 Ω cm) (10 mm × 10 mm). Prior to growth, the substrates were pretreated with N_2 plasma at 650 W at 40 Torr while the substrate temperature was maintained at 900 °C. Synthesis was then carried out using CH_4/N_2 (gas flow

ACS Publications   © XXXX American Chemical Society

A

dx.doi.org/10.1021/jp110476m | *J. Phys. Chem. C* XXXX, XXX, 000–000

ratio = 1:4) plasma at 800 W for a duration of 60 s. The samples were allowed to cool under a constant N_2 flow. The conditions used were similar to the ones used in our previous publication.[14]

Further N_2 plasma treatment of samples was carried out using a low-pressure, room-temperature in situ ECR plasma treatment. The ECR treatment offers the advantages of high dissociation percentage of process gas and high uniformity of plasma energy over large areas. The chamber was pumped down to a base pressure better than 7×10^{-5} Torr using a combination of a turbo molecular pump (TMP) and a rotary pump. The condition at which resonance occurs for electrons is a function of the excitation frequency of the alternating electric field and the strength of the static magnetic field. In our system, as mentioned before, the excitation source is 2.45 GHz and the strength of the static magnetic field is 875 G. For sufficient resonance to occur, the process pressure should be sufficiently low. For N doping, we have used a working pressure of ~0.025 Pa (1.8×10^{-4} Torr) and the microwave power was maintained at 150 W for a duration of 5 min.

Scanning electron microscopy (SEM) was performed on a FEI Quanta 3D operating at 30 kV. High-resolution TEM (HRTEM) analysis was performed on a JEOL JEM-4000EX operating at 100 kV, for which samples were scraped off the surface and deposited on 300-mesh holey carbon grids. Raman spectroscopy was performed using an ISA LabRam system equipped with a 632.8 nm He—Ne laser with a spot size of ~2—3 μm, yielding a spectral resolution of better than 2 cm^{-1}. Due care was given to minimize sample heating by using a low laser power below 2 mW. FE studies were measured in a high-vacuum chamber with a parallel diode type configuration with a base pressure around 1.5×10^{-6} Torr. The anode is made up of a copper rod with a length of 18.0 cm and diameter of 1.8 cm that was attached directly to the micrometer with a least count of 10 μm and fixed on top of the high-vacuum chamber. The cathode plate has a diamter of 6.0 cm in the middle of which a substrate holder with a height of 0.5 cm and diameter of 1.0 cm was used for mounting the sample. The samples were fixed to the cathode sample holder using silver epoxy to ensure good electrical contact. The anode—cathode distance was adjusted by a micrometer screw (attached to the anode) controlled from outside the chamber. The samples were subjected to multiple cycles of voltage sweeps until stable emission characteristics were obtained. The emission current was measured by sweeping the voltages using an automatically controlled Keithley 6514 electrometer and SRS power supply (model PS-325). For FE stability measurements, 2400 data points were collected each 5 s apart with an acquistion time of approximately 3 h.

RESULTS AND DISCUSSION

Microstructure of FLGs. Figure 1a,b shows the SEM images of as-grown and N-doped FLGs, where the vertical alignment to the substrate can be clearly observed. The vertically aligned orientation is a unique feature of the MPECVD synthesis route, and as mentioned before, it provides an excellent structure for direct investigation of field emission behavior. No discernible differences between the pristine and the N_2 plasma-treated FLGs could be made out in the SEM images at these magnifications. As observed here and demonstrated previously as well, the FLGs present a robust netlike structure with a high degree of interweaving, which increases with the increase in growth time.[14]
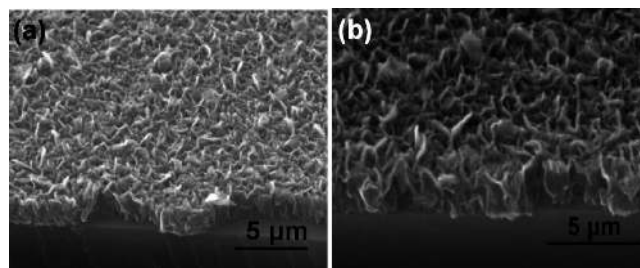

Figure 1. SEM images of (a) pristine and (b) N-doped FLGs.

The TEM analysis of pristine samples confirmed that the flakes are made up of a large number of graphitic edges and graphitic planes. The low-magnification image (Figure 2a) shows a crumpled sheetlike morphology with a thick base several hundred nanometers wide constantly narrowing down along the axial direction, where the structure is terminated with 1—3 layers of graphene at the top.[14] For N-doped samples, the high-magnification image confirms the structural and morphological changes occurring upon plasma treatment. Incorporation of nitrogen in graphene and graphene-based nanostructures, such as carbon nanotubes, has been studied extensively.[10,11] It has been shown that the incorporation of nitrogen into graphite-like structures introduces pentagonal defects in the hexagonal structure of the graphene sheets.[10] The formation of pentagons creates distortion and bending of graphite layers, leading to graphene sheets with high curvatures and cross-linked structures.[10,11] We have observed similar effects of nitrogen doping in our samples. High-resolution images of pristine FLGs show that the basal planes are straight and parallel to each other, as shown in Figure 2c. The N-doping by ECR plasma changes the structure dramatically, as observed in Figure 2b,d. The original parallel basal planes of the FLGs get severely distorted and appear buckled with huge fluctuations in the interplanar spacing, as confirmed by the line profiles taken across the highlighted areas shown in the insets of Figure 2c,d.

RAMAN SPECTROSCOPY

Raman spectroscopy is one of the most powerful nondestructive techniques for characterization of carbon materials. Typical Raman spectra of FLGs exhibit at least three to four major bands, denoted as D (~1330 cm^{-1}), G (~1580 cm^{-1}), D(~1620 cm^{-1}), and (2D) (~2660 cm^{-1}) band.[14−19] The defect peak intensity, D, does not have any dependence on the number of graphene layers but strictly depends on the amount of disorder present in the structure.[15−19] The G peak corresponds to the stretching vibration mode, E_{2g} phonon at the Brillouin zone center, Γ. The D peak originates from the symmetry breaking due to the finite sp^2 crystallite size and appears as a shoulder of the G band.[18,19] The (2D) peak is the second order of the D peak, which originates via a participation of two phonons with opposite wave vectors (q and $-q$), leading to momentum conservation. The appearance of the (2D) band does not require defects for its activation and is thus always present for crystalline carbon materials.[18,19] For analysis of the band shapes and full width at half-maximum (fwhm) parameters, the Raman spectra were fitted using Lorentzian peak shapes for the D, G, and (2D) bands, and a Gaussian peak for the D band.[20]

Figure 3a shows the comparative Raman spectra of pristine and N_2 plasma-treated FLGs. For pristine samples grown at 60 s, the fhwm of the G band is nearly 23.8 cm^{-1}, indicative that FLGs have a high degree of graphitization. Also, the fwhm of the (2D)
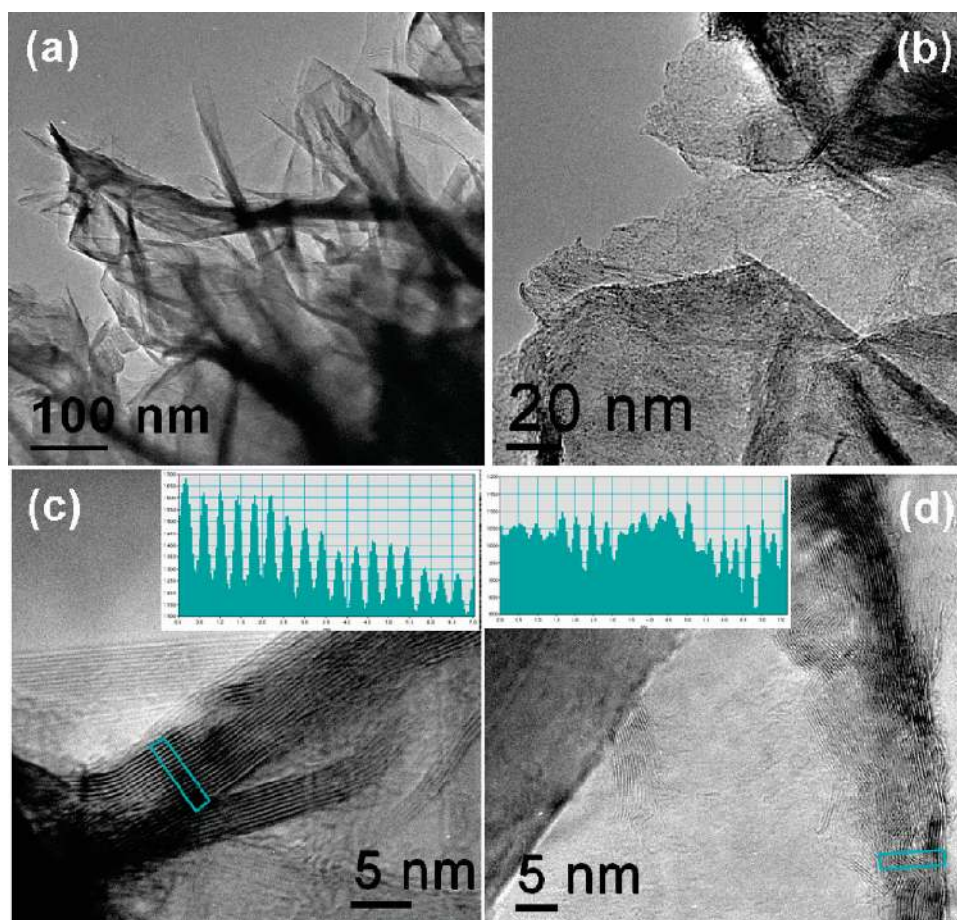
Figure 2. TEM images of (a) pristine FLGs and (b) N-doped FLGs. HRTEM images showing (c) regular and parallel basal planes in pristine FLGs and (d) distortion and buckling of planes in N-doped FLGs. Insets show planar spacing line profiles from highlighted areas.
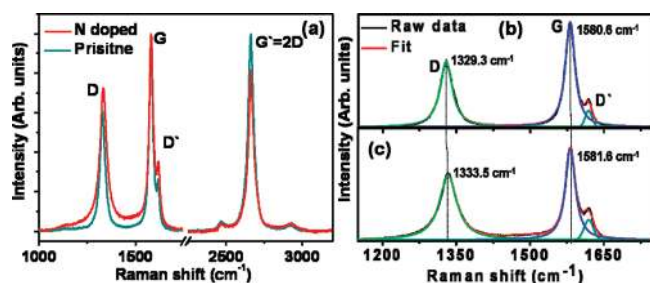

Figure 3. (a) Raman spectra of pristine and N-doped FLGs. Deconvolution of first-order Raman spectra of pristine FLGs (b) and N-doped FLGs (c). The upshift of the D and G bands upon N-doping is shown by the dotted line.

band along with the absence of graphitic shoulder is one of the indicators of an FLG system.[5,14,21] In the present study, the fwhm of the (2D) band is around 43.3 cm^{-1}, which lies within the range of 35−50 cm^{-1} observed for few-layered graphene systems.[14,21−23] For the qualitative analysis of carbon nanostructures, the value of I_D/I_G is considered as the quality factor, and ideally for highly oriented pyrolytic graphite (HOPG), this value should be zero. For pristine FLG nanoflakes grown at 60 s, the value of I_D/I_G obtained is around 0.63, whereas the $I_G/I_{(2D)}$ ratio is nearly 1. A similar nature and shape of the G band was found by Malesevic et al. in their growth of a few-layered graphene system on silicon and other metals.[5] It is also in

agreement with previous results by various authors, who have observed for chemical vapor deposition (CVD) derived few graphene layers on SiC and metals, one-, two-, and three-layered graphene samples, which all exhibit a single and sharp Lorentzian band.[24−26] The apparent high value of I_D/I_G, as compared with recent studies by other groups,[5] is caused by the high density of flakes and associated large number of edges that predominantly contribute toward the rise of a defect peak. Also, the use of longer wavelengths (low excitation energy) leads to an apparent increase of the I_D/I_G ratio.[20] However, the values of fwhm and I_D/I_G obtained are significantly smaller than those from previously reported structures, such as carbon nanowalls, nanoflakes, etc., which usually tend to show a very strong D band owing to their small crystallite size.[4] The above observations strongly support our microstructural analysis of the previous section that the synthesized material is indeed few-layered graphene.[14]

For N$_2$ plasma-treated samples, the I_D/I_G ratio increased to about 0.74 from a value of 0.63 for pristine FLGs. In addition to the differences in the I_D/I_G ratio, the spectra also exhibit a marked broadening of the Raman D band for N-doped samples (Figure 3b,c). For pristine FLGs, the D band shows a narrow fwhm of 30.7 cm^{-1}; upon N doping, this value increases to nearly 43 cm^{-1}, implying a larger distribution of the nature of defects and an enhanced defect density. In the case of the G band, the change in the fwhm was not very prominent, with a change from 23.4 to 24.5 cm^{-1}. The increase in the fwhm of the bands is in agreement with the studies of Cuesta et al.[27] that indicate that

first-order band broadening correlates strongly with the degree of graphitic disorder. Similar effects were observed by Gohel et al. in their study of N_2 plasma-treated multiwalled carbon nanotubes.[28] Along with the change in the fwhm of the bands, a slight upshift in the D band can also be observed from approximately 1329 to 1332 cm^{-1} (Figure 3b,c). This upshift in band positions has been observed previously as well and is attributed to the appearance of new and enhanced disorder in the structure.[29] The G peak position upon doping also upshifted slightly from 1580.6 to 1581.6 cm^{-1} along with the enhanced G band fwhm (Figure 3b,c). Although the G band peak shifts are more prominent in electrostatically gated monolayered graphene,[30−32] nevertheless, similar stiffening of the G band along with fwhm enhancement has been observed in chemically doped graphene by Subrahmanyam et al.[33] This blue shift of the G band (E_{2g} mode at Γ) along with the associated broadening of fwhm has been attributed to the nonadiabatic removal of the Kohn anomaly from the Brillouin zone center, Γ.[30−33] In electric field gating of graphene, by applying suitable bias, both electron and hole conduction mechanisms are accessible by shifting the Fermi level and can be observed in the upshift of the G peak in the Raman spectra for both the cases.[30,31] ECR plasma treatment induces the substitution of electron-donating nitrogen into the graphene lattice, with the overall effect of a rise in the Fermi level that is then observed in the blue shift of the G band in Raman spectra. Similar to the upshift of first-order Raman bands, the second-order Raman bands, too, show changes upon N_2 plasma treatment. The increase in the $I_G/I_{(2D)}$ value from 1 for pristine FLGs to 1.2 for N-doped FLGs is accompanied by the upshift of the (2D) band from 2661.4 to 2663.1 cm^{-1}. The blue shift of the band has been observed previously as well by Yan et al.[32] The increase in the value of $I_G/I_{(2D)}$ is an indication of increased disorder and a reduction in the overall crystallinity in N-doped FLGs and is consistent with those observed in electrostatically gated graphene.[30−32] Hence, both the first- and the second-order Raman spectra suggest an increase in the disorder of N-doped FLGs, as observed in the HRTEM studies as well as an upshift in the Fermi level, E_F, upon N doping.

■ X-RAY PHOTOELECTRON SPECTROSCOPY

The surface elemental composition of samples was examined using X-ray photoelectron spectroscopy. Figure 4a shows the wide energy survey scan (WESS) of pristine and N-doped samples. For pristine FLGs, the nominal amount of nitrogen and oxygen observed is related to sample exposure to the ambient environment. For N-doped samples, a pronounced peak near 400 eV can be clearly observed, which is attributed to the signal from N 1s states.[34] The inset of Figure 4a shows the high-resolution C 1s spectra for pristine and N-doped samples. Post N_2 plasma treatment, the C 1s signal broadens and becomes more asymmetric on the higher binding energy side. For pristine FLGs, the fwhm of the C 1s band is close to 0.56 eV, which is commensurate with that of nondoped highly crystalline sp^2 carbon, such as the highly oriented pyrolytic graphite (HOPG) value of 0.56 eV.[35] For N-doped FLGs, the fwhm of the C 1s band increases to around 0.68 eV, which can be attributed to a number of factors. In conductive materials, core−hole screening imparts an inherent line asymmetry in the XPS spectra, and an increased asymmetry of the C 1s peak of N-doped FLGs may denote a change in the electronic DOS.[35−37] In the case of CNTs, it is well known that the increase in the population of states in the
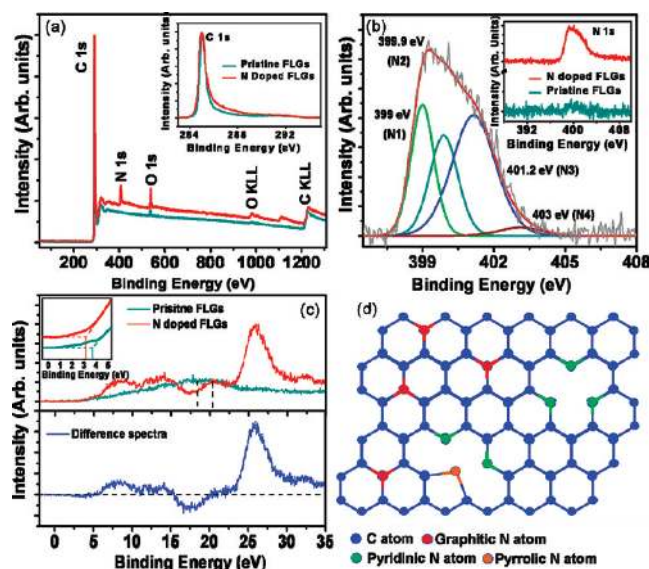

Figure 4. (a) WESS of pristine and N-doped FLGs; the inset shows the change in the high-resolution C 1s spectra. (b) Deconvolution of high-resolution N 1s spectra of N-doped FLGs; the inset shows the change in the high-resolution N 1s spectra. (c) Valence band spectra for pristine and N-doped FLGs; the lower spectrum shows the difference between the two spectra. The inset shows the change in the work function. (d) Schematic representation of N doping in graphene.

Table 1. XPS Quantification Results for Pristine and N-Doped FLGs

	element		
	atm. concentration % ± standard deviation		
sample	C	O	N
pristine FLGs	98.82 ± 0.30	0.49 ± 0.30	0.69 ± 0.22
N-doped FLGs	90.64 ± 0.21	3.06 ± 0.44	6.29 ± 0.24

electronic band gap produces carbons with enhanced metallic/conductive character.[38] Also, an increased asymmetry and broadening has also been attributed to localized lattice disorder arising from change in bonding configuration, especially a change from an sp^2 to an sp^3 bonding structure upon N doping.[39]

Table 1 shows the elemental quantification for pristine and N-doped FLG samples. It can be clearly observed that the ECR plasma treatment was successful in modifying the surface of pristine FLGs by increasing the N content from approximately 0.7 atm. % to nearly 6.3 atm. %. The increase in the nitrogen content is also accompanied by an increase in the oxygen content due to the high reactivity of functionalized sites on the graphene flakes.[40] High-resolution N 1s spectra were fitted using a Gaussian−Lorentzian mix function (ratio of 30:70) to identify the diverse chemical bonding states present in the N-doped FLGs. (Figure 4b). The N 1s spectrum was deconvoluted into four different peaks centered at 399 eV (N1), 399.9 eV (N2), 401.2 eV (N3), and 403 eV (N4). Peak N1 corresponds to a pyridinic structure in which the nitrogen atoms bond with two carbon atoms.[41−44] Peak N2 corresponds to pyrrolic-type nitrogen where nitrogen is bounded to a five member ring.[41−44] The peak N3 with a binding energy of 401.2 eV is commensurate with the presence of substitutional nitrogen in aromatic graphene.[41−44] The peak occurring at 403 eV (N4) corresponds to the presence of pyridine-N-oxide present on the surface. Figure 4d shows the various

D

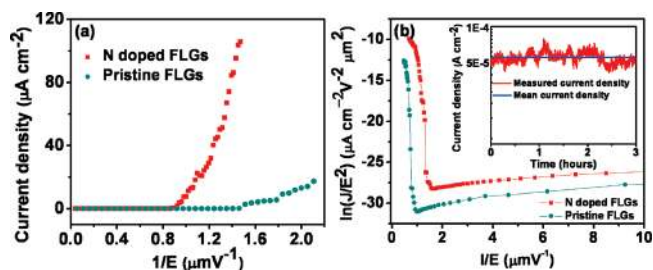dx.doi.org/10.1021/jp110476m |J. Phys. Chem. C XXXX, XXX, 000–000

Figure 5. (a) Field emission characteristics of pristine and N-doped FLGs. (b) Fowler−Nordheim plot of pristine and N-doped FLGs with stability measurement of the N-doped sample measured over a period of 3 h.

bonding configurations inserted into the graphene network upon N doping.

Figure 4c shows the normalized XPS valence band (VB) spectra of pristine and N-doped FLGs along with the difference of the two bands. Immediate observations from the valence band spectra include significant changes in the binding energy range of 5−15 eV accompanied by the appearance of new features at approximately 26 and 32 eV. The peak at 26 eV is attributed to N 2s states.[45−47] Even though the N/C atm.% ratio is only 0.07, the high intensity of the signal suggests that the photoemission cross section of N 2s and N 2p states are much higher than the carbon states.[45,48] In N-doped FLGs, the signal from the O 2s orbital at approximately 32 eV can also be observed and is related to the increased oxygen concentration upon N_2 plasma treatment, as observed in the XPS spectra as well.[47] However, the VB difference spectrum best illustrates the effect of nitrogen doping on FLGs. The difference spectrum contains positive features at 8.5 and 14 eV. The feature at 8.5 eV corresponds to changes in the C 2p σ band and may be associated with the formation of carbon nitrogen bonds.[46,47] The feature at approximately 14 eV is known to appear due to a mixture of s and p characters of the C−N bond and are typically observed in nitrogenated carbon films with a graphitic structure.[46,47] A negative feature obtained in the region between 15 and 20 eV, centered at approximately 17.5 eV, is a signature of the decrease in the number of C 2s bonds, which is consistent with an increase in the intensity of the feature at 26 eV and the formation of C−N bonds.[47,48] Also, the peak at approximately 18 eV (C 2s states) shows an upshift upon N doping to approximately 20 eV (shown by dotted lines in Figure 4c) and has been explained previously via the substitution of electron-rich nitrogen into the carbon network.[49,50] The substitution of electron-donating nitrogen into graphene sheets induces a rise in the Fermi level by introducing a donor level near the bottom of the conduction band.[8,49,50] This rise in the Fermi level corresponds to a reduction in the work function. The inset of Figure 4c shows a significant indication of the position of Fermi level E_F relative to the valence band edge. The π states are evident as a broad band in the valenece band spectra. Even though the cross section of the π electrons is low, it still is sufficient to detect their valence band.[51] In the case of pristine FLGs, the upper π band edge is located at 3.7 eV below the E_F. For N-doped FLGs, the upper edge of the π band is shifted toward the E_F and is located at nearly 3.1 eV. This difference in the photoemission threshold provides substantial evidence of a change in the work function. Thus, the VB measurements provide evidence of the rise of the Fermi level and a corresponding reduction in the work function via the formation of carbon−nitrogen bonds.

■ FIELD EMISSION

Figure 5a shows the field emission characteristics of both pristine and N-doped FLG samples. For pristine samples, the turn-on field (defined for a current density of 10 $\mu A/cm^2$) required is 1.9 V/μm, which matches well with values observed by Malesevic et al. in their report.[5] However, upon N-doping, the turn-on field is dramatically reduced to approximately 1.05 V/μm, corresponding to a reduction of nearly 94%. Also, these values are significantly better than those reported for graphene films by electophoretic deposition,[7] screen-printed graphene films,[52] carbon nanosheets,[53] carbon nanotubes,[54] and graphene nanoflakes (GNFs).[55] This reduction in turn-on voltage is accompanied by a huge enhancement of the field emission current. For pristine samples, a maximum current density of 17 $\mu A/cm^2$ was obtained at 2.16 V/μm, whereas for N-doped samples, the emission current density increased to 103 $\mu A/cm^2$ at only 1.47 V/μm.

Similar changes in the field emission behavior upon nitrogen doping in electrophoretically deposited graphene samples has been observed by Rao et al.[8] To calculate the field enhancement factor, β, we have used the following Fowler−Nordheim (FN) equation

$$J = A(\beta^2 E^2/\varphi)\exp(-B\varphi^{3/2}/\beta E) \quad (1)$$

where constant A is 1.54×10^{-10} A V^{-2} eV and constant B is 6.83×10^9 V m^{-1} $eV^{-3/2}$. The work function, φ, of FLGs is assumed to be same as that of graphite at 5 eV. The value of the field enhancement factor (β) is calculated from the slope of the high-field and low-field regions of the FN plot using the following equation

$$\beta = -(B\varphi^{3/2})/\text{slope} \quad (2)$$

Figure 5b shows the typical FN plot for both pristine and N-doped FLG samples. For prisitine FLGs, the field enhancement factors calculated are 815 and 4710 for the low-field and high-field regions, respectively. Upon N doping, the field enhancement factors increase to approximately 3120 and 17350 for the low-field and high-field regions.

Qi et al. have reported on Ar plasma treatment on FLGs for enhancement of their FE characteristics.[6] Whereas the effects of Ar treatment are predominantly physical in nature, the effects of N_2 plasma treatment are more complex in nature. In our case, the enhancement of field emission after N doping can be attributed to both physical and chemical changes that occur during the ECR treatment as well as the electrode geometry. As observed previously from Raman measurements, microstructural changes occur upon plasma treatment, which increases the effective number of defects present in the structure. It has been reported previously that the increase in the number of defects can lead to higher field emission current.[46,51] It is known that a considerable increase in β can be attributed to the change in the geometrical parameters of the field emission sites and, in particular, to the radius of curvature and the number density on the substrate.[6] Upon N doping, the almost perfect basal planes of FLGs are transformed into much more curved and bent layers. These local distortions with high curvature can act as effective sites for electron emission. Because the field amplification factor, β, at these sites is much higher, the overall effect of this is such that the N-doped FLGs can have a higher β value for both the low-field and the high-field regions.[11] However, this change in defect density and local perturbations is not the only reason for

enhanced field emission. The chemical changes that occur upon plasma treatment need to be taken into account as well.

Upon nitrogen plasma treatment, nitrogen atoms can incorporate into the honeycomb graphene matrix and it is possible for them to substitute carbon atoms due to similarities in their atomic radii (Figure 4d). One excess electron is supplied upon the substitution of a carbon atom by the nitrogen atom, which increases the electron concentration in the conduction band. Although nitrogen doping has been shown to shift the Fermi level to higher binding energy, thereby reducing the work function, the grafted functionalities play an important role in deciding the sample behavior.[49] In the case of nitrogen-doped carbon nanotubes, it has been previously reported that substitutional doping enhances the field emission properties, whereas pyridinic substitution produces a degradation in the field emission properties.[11,56] In our case, the amount of substitutional doping is nearly twice that of pyridinic doping (based upon the area under the peaks), which results in the enhanced field emission properties observed via a reduction in the work function. The abundance of appropriate substitutional nitrogen doping sites along with effective changes in the electronic DOS and reduction in the work function of the doped FLGs improves the field emission properties as observed in Figure 5a. Thus for FLGs, the enhancement of electron concentration by nitrogen doping provides a route to enhanced and stabilized field emission. These results are in agreement with those observed for CNTs.

The stability of the field emission current along with the low turn-on fields are attractive prepositions for vacuum devices. The inset of Figure 5b shows the stability of the field emission current measured over 10 000 s for N-doped samples. For N-doped samples, a starting emission current of 50 μA was initiated at approximately 1.27 V/μm. It can be clearly observed that there are very little fluctuations of the order of $\pm 10.7\%$ recorded over the 3 h period, with the measured current dropping by just 6% of the initial value. Even though the N-doped FLGs show decreased crystallinity as compared with pristine FLGs, they provide superior stability. For these samples, the short-term instability observed is due to adsorption and desorption of residual gas molecules and adsorbed species. In N-doped FLGs, the plasma treatment may produce films that are essentially more uniformly distributed in emission centers, and consequently, a more uniform and stable field emission is observed. Also, the enhancement of the surface defects upon N-doping can produce defect sites across the FLG sample surface, contributing toward the field emission current. Thus, due to an even distribution of the emitting sites via N-doping, a stable field emission behavior is observed.

CONCLUSION

The valence band spectra and surface defects of pristine FLGs were considerably altered after N doping. A decrease of the work function was observed from the N-doped sample. The field emission behavior of vertically aligned pristine and N$_2$ plasma-treated FLGs has been studied. Whereas pristine FLGs are found to field emit at approximately 1.9 V/μm, N$_2$ plasma-treated FLGs showed a much lower turn-on field of approximately 1.05 V/μm. Also, on N-doped FLGs, the maximum current density observed was nearly 103 μA cm^{-2} at 1.45 V μm^{-1}, whereas on prisitine FLGs, the current density obtained was 17 μA cm^{-2} at 2.16 V μm^{-1}. This enhancement can be attributed to an increase in the surface defects, as confirmed by Raman spectroscopy and TEM studies along with the changes, such as shifting of the Fermi level to higher binding energies and a consequential reduction in the work function, confirmed by VB-XPS as well as Raman spectroscopy. The combined effect of these factors leads to an enhanced field emission response and enhanced stability from N$_2$ plasma-treated FLGs. The above results suggest that nitrogen-doped few-layered graphene nanoflakes (FLGs) have great potential as high-performance field emitters.

AUTHOR INFORMATION

Corresponding Author
*E-mail: s.sinha-roy@ulster.ac.uk.

ACKNOWLEDGMENT

REFERENCES

(1) Amaratunga, G. A. J.; Silva, S. R. P. *Appl. Phys. Lett.* **1996**, *68*, 2529–2531.

(2) Zhu, W.; Bower, C.; Zhou, O.; Kochanski, G.; Jin, S. *Appl. Phys. Lett.* **1999**, *75*, 873.

(3) Li, J. J.; Gu, C. Z.; Wang, Q.; Xu, P.; Wang, Z. L.; Xu, Z.; Bai, X. D. *Appl. Phys. Lett.* **2005**, *87*, 143107.

(4) Wu, Y.; Yang, B.; Zong, B.; Sun, H.; Shen, Z.; Feng, Y. *J. Mater. Chem.* **2004**, *14*, 469–477.

(5) Malesevic, A.; Kemps, R.; Vanhulsel, A.; Chowdhury, M. P.; Volodin, A.; Van Haesendonck, C. *J. Appl. Phys.* **2008**, *104*, 084301.

(6) Qi, J.; Wang, X.; Zheng, W.; Tian, H.; Hu, C.; Peng, Y. *J. Phys. D: Appl. Phys.* **2010**, *43*, 055302.

(7) Wu, Z. S.; Pei, S.; Ren, W.; Tang, D.; Gao, L.; Liu, B.; Li, F.; Liu, C.; Cheng, H. M. *Adv. Mater.* **2009**, *21*, 1756–1760.

(8) Palnitkar, U. A.; Kashid, R. V.; More, M. A.; Joag, D. S.; Panchakarla, L. S.; Rao, C. N. R. *Appl. Phys. Lett.* **2010**, *97*, 063102.

(9) Novoselov, K.; Jiang, D.; Schedin, F.; Booth, T. J.; Khotkevich, V. V.; Morozov, S. V.; Geim, A. K. *Proc. Natl. Acad. Sci. U.S.A.* **2005**, *102*, 10451–10453.

(10) Ahn, H. S.; Lee, K. R.; Kim, D. Y.; Han, S. *Appl. Phys. Lett.* **2006**, *88*, 093122.

(11) Chan, L. H.; Hong, K. H.; Xiao, D. Q.; Hsieh, W. J.; Lai, S. H.; Shih, H. C.; Lin, T. C.; Shieu, F. S.; Chen, K. J.; Cheng, H. C. *Appl. Phys. Lett.* **2003**, *82*, 4334.

(12) Cervantes-Sodi, F.; Csanyi, G.; Piscanec, S.; Ferrari, A. *Phys. Rev. B* **2008**, *77*, 165427.

(13) Deifallah, M.; McMillan, P. F.; Cora, F. *J. Phys. Chem. C* **2008**, *112*, 5447–5453.

(14) Soin, N.; Roy, S. S.; O'Kane, C.; Lim, T. H.; Hetherington, C. J. D.; McLaughlin, J. A. *CrystEngComm* **2011**, *13*, 312–318.

(15) Ferrari, A. C.; Robertson, J. *Phys. Rev. B* **2000**, *61*, 14095–14107.

(16) Tuinstra, F.; Koenig, J. L. *J. Chem. Phys.* **1970**, *53*, 1126–1130.

(17) Ferrari, A. C.; Robertson, J. *Phys. Rev. B* **2001**, *64*, 075414.

(18) Kastner, J.; Pichler, T.; Kuzmany, H.; Curran, S.; Blau, W.; Weldon, D. N.; Delamesiere, M.; Draper, S.; Zandbergen, H. *Chem. Phys. Lett.* **1994**, *221*, 53–58.

(19) Casiraghi, C.; Hartschuh, A.; Qian, H.; Piscanec, S.; Georgi, C.; Fasoli, A.; Novoselov, K. S.; Basko, D. M.; Ferrari, A. C. *Nano Lett.* **2009**, *9*, 1433–1441.

(20) Soin, N.; Roy, S. S.; Ray, S. C.; McLaughlin, J. A. *J. Raman Spectrosc.* **2010**, *41*, 1227–1233.

(21) Ferrari, A. C.; Meyer, J. C.; Scardaci, V.; Casiraghi, C.; Lazzeri, M.; Mauri, F.; Piscanec, S.; Jiang, D.; Novoselov, K. S.; Roth, S.; Geim, A. K. *Phys. Rev. Lett.* **2006**, *97*, 187401.

(22) Pimenta, M. A.; Dresselhaus, G.; Dresselhaus, M. S.; Cancado, L. G.; Jorio, A.; Saito, R. *Phys. Chem. Chem. Phys.* **2007**, *9*, 1276–1290.

(23) Lee, Y.-H.; Lee, J.-H. *Appl. Phys. Lett.* **2009**, *95*, 143102–143104.

(24) Reina, A.; Jia, X.; Ho, J.; Nezich, D.; Son, H.; Bulovic, V.; Dresselhaus, M. S.; Kong, J. *Nano Lett.* **2009**, *9*, 30–35.

(25) Lee, D. S.; Riedl, C.; Krauss, B.; Klitzing, K.; von; Starke, U.; Smet, J. H. *Nano Lett.* **2008**, *8*, 4320–4325.

(26) Ismach, A.; Druzgalski, C.; Penwell, S.; Schwartzberg, A.; Zheng, M.; Javey, A.; Bokor, J.; Zhang, Y. *Nano Lett.* **2010**, *10*, 1542–1548.

(27) Cuesta, A.; Dhamelincourt, P.; Laureyns, J.; Martinez-Alonso, A.; Tascon, J. M. D. *Carbon* **1994**, *32*, 1523–1532.

(28) Gohel, A.; Chin, K. C.; Zhu, Y. W.; Sow, C. H.; Wee, A. T. S. *Carbon* **2005**, *43*, 2530–2535.

(29) Yang, Q. H.; Hou, P. X.; Unno, M.; Yamauchi, S.; Saito, R.; Kyotani, T. *Nano Lett.* **2005**, *5*, 2465–2469.

(30) Pisana, S.; Lazzeri, M.; Casiraghi, C.; Novoselov, K. S.; Geim, A. K.; Ferrari, A. C.; Mauri, F. *Nat. Mater.* **2007**, *6*, 198–201.

(31) Das, A.; Pisana, S.; Chakraborty, B.; Piscanec, S.; Saha, S. K.; Waghmare, U. V.; Novoselov, K. S.; Krishnamurthy, H. R.; Geim, A. K.; Ferrari, A. C.; Sood, A. K. *Nat. Nanotechnol.* **2008**, *3*, 210–215.

(32) Yan, J.; Zhang, Y.; Kim, P.; Pinczuk, A. *Phys. Rev. Lett.* **2007**, *98*, 166802.

(33) Subrahmanyam, K. S.; Panchakarla, L. S.; Govindraj, A.; Rao, C. N. R. *J. Phys. Chem. C* **2009**, *113*, 4257–4259.

(34) Briggs, D.; Grant, J. T. *Surface Analysis by Auger and X-ray Photoelectron Spectroscopy*; IM Publications and Surface Spectra Limited: Chichester, U.K., 2003.

(35) Leiro, J. A.; Heinonen, M. H.; Laiho, T.; Batirev, I. G. *J. Electron Spectrosc. Relat. Phenom.* **2003**, *128*, 205–213.

(36) Sette, F.; Wertheim, G. K.; Ma, Y.; Meigs, G. *Phys. Rev. B* **1990**, *41*, 9766–9770.

(37) Maldonado, S.; Morin, S.; Stevenson, K. J. *Carbon* **2006**, *44*, 1429–1437.

(38) Terrones, M.; Ajayan, P. M.; Banhart, F.; Blase, X.; Carroll, D. L.; Charlier, J. C.; Czerw, R.; Foley, B.; Grobert, N.; Kamalakaran, K. *Appl. Phys. A: Mater. Sci. Process.* **2002**, *74*, 355–361.

(39) Estrade-Szwarckopf, H. *Carbon* **2004**, *42*, 1713–1721.

(40) Abbas, G.; Papakonstantinou, P.; Iyer, G. R. S.; Kirkman, I. W.; Chen, L. C. *Phys. Rev. B* **2007**, *75*, 195421–195429.

(41) Choi, H. C.; Bae, S. Y.; Jang, W.; Park, J.; Song, H. J.; Shin, H.; Jung, H.; Ahn, J. *J. Phys. Chem. B* **2005**, *109*, 1683–1688.

(42) Kapteijn, F.; Moulijn, J. A.; Matzner, S.; Boehm, H. P. *Carbon* **1999**, *37*, 1143–1150.

(43) Kundu, S.; Nagaiah, T. C.; Xia, W.; Wang, Y.; Dommele, S. V.; Bitter, J. H.; Santa, M.; Grundmeier, G.; Bron, M.; Schuhmann, W.; Muhler, M. *J. Phys. Chem. C* **2009**, *113*, 14302–14310.

(44) Choi, J.-Y.; Hsu, R. S.; Chen, Z. *J. Phys. Chem. C* **2010**, *114*, 8048–8053.

(45) Choi, H. C.; Park, J.; Kim, B. *J. Phys. Chem. B* **2005**, *109*, 4333–4340.

(46) Ray, S. C.; Pao, C. W.; Tsai, H. M.; Chiou, J. W.; Pong, W. F.; Chen, C. W. *Appl. Phys. Lett.* **2007**, *90*, 192107.

(47) Bhattacharyya, S.; Spaeth, C.; Richter, F. *J. Appl. Phys.* **2001**, *89*, 2414–2421.

(48) Zhao, J. P.; Chen, Z. Y.; Yano, T.; Ooie, T.; Yoneda, M.; Sakakibara, J. *J. Appl. Phys.* **2001**, *89*, 1634–1640.

(49) Santos, M. C.; dos Alvarez, F. *Phys. Rev. B* **1998**, *58*, 13918–13924.

(50) Lim, S. H.; Elim, H. I.; Gao, X. Y.; Wee, A. T. S.; Ji, W.; Lee, J. Y.; Lin, J. *Phys. Rev. B* **2006**, *73*, 45402.

(51) Glenis, S.; Nelson, A. J.; Labes, M. M. *J. Appl. Phys.* **1996**, *80*, 5404–5408.

(52) Qian, M.; Feng, T.; Ding, H.; Lin, L.; Li, H.; Chen, Y.; Sun, Z. *Nanotechnology* **2002**, *20*, 425702.

(53) Wang, J. J.; Zhu, M. Y.; Outlaw, R. A.; Zhao, X.; Manos, D. M.; Holloway, B. C. *Appl. Phys. Lett.* **2004**, *85*, 1265–1267.

(54) Shang, N. G.; Li, C. P.; Wong, W. K.; Lee, C. S.; Bello, I.; Lee, S. T. *Appl. Phys. Lett.* **2002**, *81*, 5024–5026.

(55) Pao, C. W.; Ray, S. C.; Tsai, H. M.; Chen, Y. S.; Chen, H.-C.; Lin, I.-N.; Pong, W. F.; Chio, J. W.; Tsai, M.-H.; Shang, N. G.; Papakonstantinou, P.; Guo, J.-H. *J. Phys. Chem. C* **2010**, *114*, 8161–8166.

(56) Ghosh, K.; Kumar, M.; Maruyama, T.; Ando, Y. *Carbon* **2010**, *48*, 191–200.